

COVER PAGE

Document downloaded by @DAEL

Thu Nov 26 16:20:49 2026
For personal use

When automatic English translation is provided, only the original document is authentic.
The EAA cannot be held responsible of any translation error

Bibliographical reference

Ultrasounds Excited by a Laser Line Pulse in a Liquid-Filled Tube, Y. Pan, N. Chigarev, B. Audoin and C. Rossignol, Acta Acustica **vol. 94** (Number 5), 2008, pp. 694-702

DOI
https://doi.org/10.3813/AAA.918083

ACTA ACUSTICA UNITED WITH ACUSTICA
Vol. 94 (2008) 694 – 702

DOI 10.3813/AAA.918083

Ultrasounds Excited by a Laser Line Pulse in a Liquid-Filled Tube

Y. Pan
Institute of Acoustics, Tongji University, 200092, Shanghai, P. R. China. ypan@mail.tongji.edu.cn

N. Chigarev, B. Audoin, C. Rossignol
Laboratoire de Mécanique Physique, UMR CNRS 8469, Université Bordeaux 1, 33405 Talence, France

Summary
In this paper, a physical model is proposed to describe the propagation of ultrasounds, which are excited in a homogeneous, isotropic, and liquid-filled tube by a laser line source under either the ablation or thermoelastic regime. Since a metal tube is considered, the thermal diffusion and the optical penetration depth are neglected in this modeling. The Fourier series expansion is introduced for a spatial coordinate to provide the transient response of the structure. Theoretical displacements are obtained for aluminum tubes filled with glycerol or air. The corresponding displacements are observed experimentally by the laser ultrasonic technique. Good agreement is found in the arrival time, shape and relative amplitude of various longitudinal and shear bulk waves propagating in the solid and liquid media. These ultrasonic waves are further identified by the ray trajectory analysis.

PACS no. 43.35.Cg, 43.35.Zc, 43.20.Bi

1. Introduction

Materials with the hollow cylindrical structure are extensively applied in industries, such as pipelines for gas and oil. Since one failure of such a structure may cause serious consequences, there is an obvious need for their nondestructive evaluation (NDE) to avoid any possible failure. The understanding of the wave generation and propagation in such a unique geometry is thus of large interest for the acoustic research community. Deep analysis of the intrinsic rich information in the transient response should deepen the current understanding of the ultrasounds excitation and propagation in cylindrical structures.

Early in 1952, Junger and Mass [1] have studied the coupled vibrations of fluid-filled cylindrical shells. They have found the frequency equation, i.e. the characteristic or dispersion equation for harmonic elastic waves. In 1959, Gazis [2] has investigated theoretically the wave propagation in an empty tube. He got the dispersion equation for harmonic waves propagating along the circumferential, axial, or helical direction, and some dispersion curves were numerically obtained. In 1989, Plona *et al.* [3] have investigated experimentally the wave propagation in a fluid-filled tube, and dispersion was observed in agreement to the theory. Still, several works are examining such wave propagation. For instance, Zhao and Rose [4] have recently studied the shear horizontal waves propagating along the circumferential direction for an empty tube.

Received 23 February 2008,
accepted 3 September 2008.

For a NDE purpose, Liu and Qu [5] have calculated the transient wave propagation along the circumferential direction by applying normal mode expansion (NME) method, and they have analyzed the influence of the incident angle of a PZT transducer for generation and detection. But the corresponding experimental result is hard to obtain due to the difficulty of coupling the transducer to the cylinder. The laser ultrasonic technique [6] is better suited, since the transient waves can be generated and detected at a distance, without any contact to the sample. Good agreement between experiment and theory has been found for aluminum rods excited by laser line source under either ablation or thermoelastic regime [7]. These laser excited ultrasounds were successfully predicted and identified as various bulk and surface waves with their corresponding ray trajectories [8]. To further demonstrate the advantage of the laser ultrasonic technique, the laser generated transient waves propagating along the axial and helical directions were numerically analyzed by Tang and Cheng [9] recently.

Also for a NDE purpose, Gao *et al.* [10] have excited ultrasounds propagating along the circumferential direction to study the interactions with possible defects in both inner and outer cylindrical surfaces of a tube. But since the thickness of the studied tube was relatively small, only guided waves were experimentally observed and studied.

Very recently, the authors [11] have developed a physical model and theoretical solution to predict the propagation along the circumferential direction of the transient wave generated by a laser line pulse in an empty tube, and good agreement between experiment and theory was

© S. Hirzel Verlag · EAA

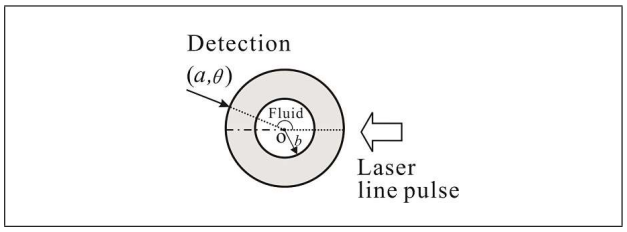

Figure 1. Problem geometry.

found for various bulk and surface waves including guided waves.

The acoustic scattering of an immersed tube in water was also under the scope of several research works. For instance, Kim and Ih [12] have investigated theoretically and experimentally the air-filled water-immersed transversely isotropic tube to characterize its elastic constants. Wilson *et al.* [13] have studied the acoustic scattering by a tube filled with a bubbly liquid and immersed in water under a very low frequency range for a possible application in sea. To the best of author's knowledge, in the literature no work has been performed on the transient wave propagation for a liquid-filled tube under laser impacts.

In this paper, a physical model and corresponding theoretical solution are presented to predict ultrasounds excited in a fluid-filled tube by a pulsed laser line source under either ablation or thermoelastic generation. Numerical radial displacements, on the surfaces of aluminum tubes filled with air or glycerol, are presented and analyzed for various ratios of internal radius to external radius. Experimental displacements were detected by the laser ultrasonic technique under either ablation or thermoelastic regime. Theoretical responses are calculated and compared with the corresponding experimental results.

2. General formulation

Let us consider a homogenous and isotropic tube of infinite length, density ρ, external and internal radii a and b, respectively. The tube is filled with a fluid of density ρ_F. The symmetry axis of the cylinder is assumed to coincide with the z-axis of the system of cylindrical coordinates (r, θ, z). A pulsed laser beam, focused along the z-axis by a cylindrical lens, impacts the tube to excite ultrasounds. As shown in Figure 1, the focused laser beam provides a line-like acoustic source at the position $\theta = 0°$. The excited ultrasounds are experimentally observed with an optical interferometric detection technique [8, 14]. To define the point detection position, the cylindrical coordinates (a, θ) are chosen, considering $\theta = 0°$ and $r = a$ for the source position.

Let λ and μ denote the two independent Lamé coefficients of the isotropic material of the tube, and let $\rho_F^{-1} V_F^{-2})$ (V_F is the ultrasound velocity in the fluid) represent the compressibility of the fluid. Assuming an infinitely long line-source, the problem shows invariance along the z-direction. The non-zero components of the displacement vector depend on two spatial variables r, θ and on time t. Let u_r, u_θ denote the radial and tangential components of the displacement vector in the solid, and u_F stand for the radial component in the fluid. The circumferential component in the fluid, although not equal to zero, is not considered explicitly in the following. These components can be expressed in terms of three scalar potentials $\varphi(r, \theta, t)$, $\psi(r, \theta, t)$ and $\chi(r, \theta, t)$ as

$$\begin{aligned} u_r(r,\theta,t) &= \frac{\partial \varphi}{\partial r} + \frac{1}{r}\frac{\partial \psi}{\partial \theta}, \\ u_\theta(r,\theta,t) &= \frac{1}{r}\frac{\partial \varphi}{\partial \theta} - \frac{\partial \psi}{\partial r}, \\ u_F(r,\theta,t) &= \frac{\partial \chi}{\partial r}, \end{aligned} \tag{1}$$

where these potentials are governed by the following three wave motion equations

$$\begin{aligned} \frac{\partial^2 \varphi}{\partial r^2} + \frac{1}{r}\frac{\partial \varphi}{\partial r} + \frac{1}{r^2}\frac{\partial^2 \varphi}{\partial \theta^2} &= \frac{\rho}{\lambda + 2\mu}\frac{\partial^2 \varphi}{\partial t^2}, \\ \frac{\partial^2 \psi}{\partial r^2} + \frac{1}{r}\frac{\partial \psi}{\partial r} + \frac{1}{r^2}\frac{\partial^2 \psi}{\partial \theta^2} &= \frac{\rho}{\mu}\frac{\partial^2 \psi}{\partial t^2}, \\ \frac{\partial^2 \chi}{\partial r^2} + \frac{1}{r}\frac{\partial \chi}{\partial r} + \frac{1}{r^2}\frac{\partial^2 \chi}{\partial \theta^2} &= \frac{1}{V_F^2}\frac{\partial^2 \chi}{\partial t^2}. \end{aligned} \tag{2}$$

In equations (2), the potentials φ and ψ represent the harmonic wave propagation of the pure longitudinal (L) and vertically polarized pure shear (S) waves in the solid part of the tube, respectively. And the potential χ represents the harmonic wave propagation of the pure compressive (F) wave in the liquid filling the tube. To further address the transient wave excitation and propagation, the two potentials φ and ψ must satisfy the following boundary conditions at the surface ($r = a$). For a source at position $\theta = 0°$ and $z = 0$, components σ_{rr} and $\sigma_{r\theta}$ of the stress tensor at any point of the cylinder surface are determined by either

$$\sigma_{rr}|_{r=a} = -\sigma_A\, \delta_A(t)\, \delta(\theta), \quad \sigma_{r\theta}|_{r=a} = 0 \tag{3}$$

for the ablation generation [15], or

$$\sigma_{rr}|_{r=a} = 0, \quad \sigma_{r\theta}|_{r=a} = -\sigma_T\, h(t)\, \delta'(\theta) \tag{4}$$

for the thermoelastic generation [16]. In equations (3) σ_A stands for the normal force magnitude in N μs/m^2, and in equations (4) σ_T is the dipole force magnitude in N/m^2. They are related to the intensity of the laser point pulse, and their magnitudes are fixed to unity for the corresponding calculations in the following sections. Here a delta function of time $\delta(t)$ and a Heaviside step function of time $h(t)$ are used for the ablation and thermoelastic generations, respectively; $\delta'(\theta)$ denotes the derivative of the delta function $\delta(\theta)$. In equations (3), a delta force is postulated in time and space to represent the sudden normal loading in the ablation regime [15]. In equations (4), a Heaviside step function in time is considered in the thermoelastic regime, since thermal diffusion is neglected [16]. Owing to the interface, two dipolar forces are thus considered for the source shape [17]. Here setting the range for θ from

$-\pi$ to $+\pi$ instead of from $-\infty$ to $+\infty$ also accounts for the periodicity of the cylindrical structure as presented in the following section. In addition, all three potentials must satisfy the boundary conditions at the solid–liquid interface, which are the continuity of the normal component of the displacement as well as the stress, and the vanishing of the shear components of the stress. They are expressed as

$$\begin{aligned} \sigma_{rr}|_{r=b} &= \sigma_{rr}^{F}|_{r=b}\,, \\ \sigma_{r\theta}|_{r=b} &= 0\,, \\ u_r|_{r=b} &= u_F|_{r=b}\,. \end{aligned} \tag{5}$$

3. Transformed solutions and numerical inverse scheme

To avoid the integration along the wave number ν ($\nu = k_\theta a$, where k_θ is the component of the wave vector $\boldsymbol{k}$ along the θ-direction) necessitated by the numerical inversion scheme, the Fourier series expansion is introduced for the coordinate θ. In addition, the Fourier transform is considered for time t; and the angular frequency ω is thus introduced. Doing so, the displacement field $u_i(r,\theta,t)$ ($i = r,\theta,F$) is now transformed in $U_i(r,\nu,\omega)$ as the following form

$$U_i(r,\nu,\omega) = \int_{-\infty}^{+\infty}\left(\int_{-\pi}^{+\pi} u_i(r,\theta,t)\mathrm{e}^{\mathrm{j}\nu\theta}\mathrm{d}\theta\right)\mathrm{e}^{-\mathrm{j}\omega t}\mathrm{d}t. \tag{6}$$

Applying the Fourier series expansion and the Fourier transform, the wave motion equations and the boundary equations provide explicit solution forms for the potentials φ, ψ and χ under either generation regime. At any position on the cylinder surface, the transformed displacement components $U_i(r,\nu,\omega)$ ($i = r,\theta,F$) are then obtained from equations (2), (3) and (5) for the ablation generation as

$$\begin{aligned} U_r(a,\nu,\omega) &= -\frac{\sigma_A a}{2\mu D(\nu,\omega)} \\ &\quad\cdot\left[A_1 B_L^a + A_2 Y_L^a - \mathrm{j}\nu A_3 - \mathrm{j}\nu A_4\right], \\ U_\theta(a,\nu,\omega) &= -\frac{\sigma_A a}{2\mu D(\nu,\omega)} \\ &\quad\cdot\left[\mathrm{j}\nu A_1 + \mathrm{j}\nu A_2 + A_3 B_S^a + A_4 Y_S^a\right], \\ U_F(b,\nu,\omega) &= -\frac{\sigma_A a}{2\mu D(\nu,\omega)} A_5 B_F^b, \end{aligned} \tag{7}$$

and from equations (2), (4) and (5) for the thermoelastic generation as

$$\begin{aligned} U_r(a,\nu,\omega) &= \frac{\sigma_T a H(\omega)}{2\mu D(\nu,\omega)} \\ &\quad\cdot\left[T_1 B_L^a + T_2 Y_L^a - \mathrm{j}\nu T_3 - \mathrm{j}\nu T_4\right], \\ U_\theta(a,\nu,\omega) &= -\frac{\sigma_T a H(\omega)}{2\mu D(\nu,\omega)} \\ &\quad\cdot\left[\mathrm{j}\nu T_1 + \mathrm{j}\nu T_2 + T_3 B_S^a + T_4 Y_S^a\right], \\ U_F(b,\nu,\omega) &= \frac{\sigma_T a H(\omega)}{2\mu D(\nu,\omega)} T_5 B_F^b. \end{aligned} \tag{8}$$

In equations (8), $H(\omega)$ is the Fourier transform of the Heaviside step function $h(t)$. In the above equations, parameters B_W^a, Y_W^a ($W = L, S$) and B_F^b are determined by

$$\begin{aligned} B_W^a &= k_W a J_\nu'(k_W a)/J_\nu(k_W a), \\ Y_W^a &= k_W a Y_\nu'(k_W a)/Y_\nu(k_W a), \\ B_F^b &= k_F b J_\nu'(k_F b)/J_\nu(k_F b). \end{aligned} \tag{9}$$

Here, $J_\nu'(x)$ is the derivative of $J_\nu(x)$, the Bessel function of first kind; $Y_\nu'(x)$ is the derivative of $Y_\nu(x)$, the Bessel function of second kind; $k_L = \omega/V_L = \omega\sqrt{\rho/(\lambda+2\mu)}$ and $k_F\omega/V_F$ are the wave number of the longitudinal or compressive waves for solid and fluid, with V_L and V_F the longitudinal and compressive wave velocities of solid and fluid, respectively. In addition, $k_S = \omega/V_S = \omega\sqrt{\rho/\mu}$ is the wave number of the shear wave for the solid tube, with V_S the shear wave velocity of solid.

Variables A_n and T_n ($n = 1,\ldots,5$) are given by

$$\begin{aligned} &A_1 = d_{11}, \quad A_2 = d_{12}, \quad A_3 = d_{13}, \\ &A_4 = d_{14}, \quad A_5 = d_{15}, \\ &T_1 = d_{21}, \quad T_2 = d_{22}, \quad T_3 = d_{23}, \\ &T_4 = d_{24}, \quad T_5 = d_{25}, \end{aligned} \tag{10}$$

where $\{d_{ij}\}$ are the cofactors of the following matrix

$$m_{ij} = \tag{11}$$

$$\begin{pmatrix} \nu^2 - k_S^2 a^2/2 - B_L^a & \nu^2 - k_S^2 a^2/2 - Y_L^a \\ \mathrm{j}\nu(1 - B_L^a) & \mathrm{j}\nu(1 - Y_L^a) \\ (\nu^2 - k_S^2 b^2/2 - B_L^b)B_L^e & (\nu^2 - k_S^2 b^2/2 - Y_L^b)Y_L^e \\ \mathrm{j}\nu(1 - B_L^b)B_L^e & \mathrm{j}\nu(1 - Y_L^b)Y_L^e \\ B_L^b B_L^e & Y_L^b Y_L^e \end{pmatrix} \cdots$$

$$\begin{pmatrix} \mathrm{j}\nu(1 - B_S^a) \\ k_S^2 a^2/2 - \nu^2 + B_S^a \\ \mathrm{j}\nu(1 - B_S^b)B_S^e \\ (k_S^2 b^2/2 - \nu^2 + B_S^b)B_S^e \\ -\mathrm{j}\nu B_S^e \end{pmatrix} \cdots$$

$$\begin{pmatrix} \mathrm{j}\nu(1 - Y_S^a) & 0 \\ k_S^2 a^2/2 - \nu^2 + Y_S^a & 0 \\ \mathrm{j}\nu(1 - Y_S^b)Y_S^e & \rho_F k_S^2 b^2/2\rho \\ (k_S^2 b^2/2 - \nu^2 + Y_S^b)Y_S^e & 0 \\ -\mathrm{j}\nu Y_S^e & -B_F^b \end{pmatrix}.$$

The elements in matrix $\{m_{ij}\}$ correspond to the coefficients of five linear equations (equations (3) and (5) for A_n, equations (4) and (5) for T_n ($n = 1,\ldots,5$) derived from the boundary conditions for either generation regime. In equation (11), parameters B_W^e and Y_W^e ($W = L, S$) are determined by

$$\begin{aligned} B_W^e &= J_\nu(k_W b)/J_\nu(k_W a), \\ Y_W^e &= Y_\nu(k_W b)/Y_\nu(k_W a), \end{aligned} \tag{12}$$

and parameters B_W^b and Y_W^b ($W = L, S$) can be obtained by replacing a with b in equation (9). Note that in equations (7) and (8), $D(\nu,\omega) = \det(m_{ij})$ is the determinant of the matrix $\{m_{ij}\}$ in equation (11).

The explicit forms of the displacement field for a fluid-filled tube (equations 7 and 8) can also represent that for an empty tube or a hollow cylinder. As the 4 × 4 elements in the upper-left corner of the matrix of equation (11) are identical to that in the corresponding matrix for an empty tube (equation (5) in [11], the ratios $A_i/D(\nu,\omega)$ and $T_i/D(\nu,\omega)$ $(i = 1,\ldots,4)$ are identical to that for the empty tube (see equation (6) in reference [11]), when the density of the liquid approaches zero ($\rho_F \to 0$). Therefore, the transient displacement responses at the surface are identical to that for an empty tube with $\rho_F \to 0$. Moreover, as the 5 × 5 matrix in equation (11) reduces to a 2 × 2 matrix of its upper-left corner for a rod, the corresponding explicit solutions can deliver the same solution as in the author's previous publication (see equation (6) in reference [7]). Thus, the current theoretical solutions (equations 7 and 8) could deal with the specific cases of an empty tube or even of a rod. Consequently, the results of author's previous papers support the current solutions which, of course, are more general.

Now, it is time to focus on the calculation of the displacement field over coordinates θ, and time t by the inverse form of equation (6). The calculation of the inverse form meets discontinuities for a particular set of ω and ν values. They correspond to poles associated with the zeros of the dispersion equation

$$D(\nu,\omega) = \det(m_{ij}) = 0. \tag{13}$$

When $\rho_F \to 0$, this equation addresses the dispersion of guided waves for an empty tube as studied by Liu and Qu [5]. In addition, for a rod, this equation yields to

$$\left(\nu^2 - k_S^2 a^2/2\right)^2 - \nu^2 + k_S^2 a^2\left(B_L + B_S\right)/2 + (1-\nu^2)B_L B_S = 0, \tag{14}$$

which is identical to $D_\nu = 0$ for equation (8) of [19]. These poles describe the cylindrical Rayleigh waves [18] and Whispering Gallery waves [19]. Thus the integration cannot be carried out numerically. Therefore, a small constant δ is introduced as the imaginary part for ω as discussed in the previous paper [8, 20]. With this change, the inverse form of equation (6) becomes

$$u_i(r,\theta,t) = \frac{1}{4\pi^2} e^{\delta t} \int_{-\infty}^{+\infty} \left(\sum_{\nu=-\infty}^{+\infty} U_i(r,\nu,\omega - j\delta) e^{-j\nu\theta} \right) e^{j\omega t} d\omega. \tag{15}$$

Doing so, ω becomes complex, $\omega - j\delta$, and the poles are moved off the real axis of variable ω. Now the integration can be calculated numerically. Various numerical results along with the comparison to the experimental displacements are going to demonstrate the capability of this numerical inverse scheme in the next section.

4. Ultrasounds excited in air-filled tubes

In order to demonstrate, firstly for an empty tube, the capability of the theoretical solution presented in the previous sections, the radial surface displacements are calculated for air-filled aluminum tubes with velocities of longitudinal wave $V_L = 6400\,\mathrm{m/s}$, and shear wave $V_S = 3110\,\mathrm{m/s}$, and with a density $\rho = 2700\,\mathrm{kg/m^3}$ at an observation angle θ of 180° [21]. The displacements of four air-filled tubes with outer radius $a = 5\,\mathrm{mm}$ and inner radius $b = 1, 2, 3, 4\,\mathrm{mm}$ are shown in Figure 2 for both ablation and thermoelastic generation regimes. Here the velocity and density of air are chosen to be $V_F = 344\,\mathrm{m/s}$ and $\rho_F = 1.19\,\mathrm{kg/m^3}$ at the room temperature of 20 °C for calculation of the theoretical solutions given in the latter section [21]. Accordingly with criteria given in [20], the value $\delta = 0.06\,\mathrm{rad}/\mu\mathrm{s}$ is chosen for the auxiliary pa-

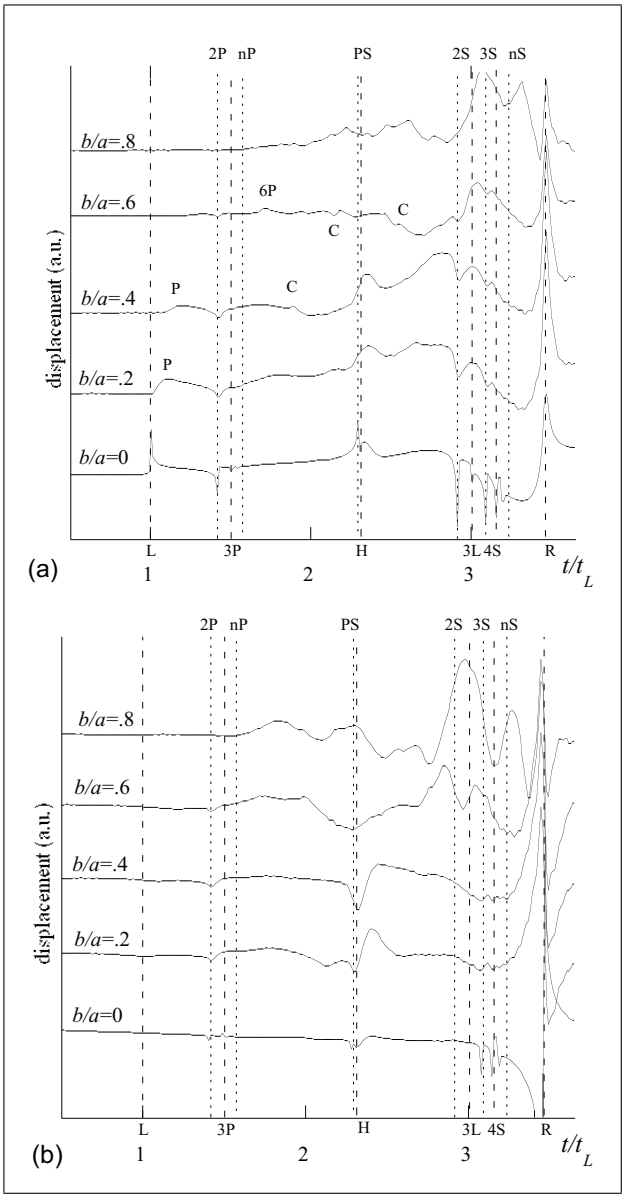

Figure 2. Displacements calculated at an observation angle θ = 180° of the laser line source generation under either the ablation (a) or the thermoelastic (b) regime for air-filled tubes with various b/a ratio of 0, 0.2, 0.4, 0.6, and 0.8. Symbols at the top or bottom of each dashed line respectively denote the wave marked by the dense or sparse dashed line.

rameter in the numerical calculations. The corresponding responses of a cylindrical rod ($a = 5$ mm and $b = 0$ mm) are calculated with the previous model [8] for the purpose of comparison.

The time scale is made dimensionless by dividing the time t by a factor t_L ($t_L = 2a/V_L$), the transit time of the direct longitudinal wave for this position of an observation angle θ of 180°. It favors the comparison, since the time scale remains unchanged for the same material with a different size. Moreover, a pair of sparse and dense dashed lines is repeatedly displayed to indicate the time arrivals of various waves summarized in Table I. The arrival time of each wave is calculated according to the corresponding ray trajectory. Every dimensionless time of flight is also listed in Table I. Symbols at the top or bottom of each pair of dash lines respectively represent the name of the wave marked by either the dense or sparse dashed line. This representation holds for the similar figures through this paper.

First, interest is focused on ultrasounds excited under the ablation regime, as shown in Figure 2a. For every ratio (b/a increases from 0 to 0.8), the cylindrical Rayleigh wave R, also listed in Table I, is clearly visible with a large amplitude. To better visualize bulk waves with small amplitudes, the shape of each Rayleigh wave is not displayed in totality. But it is still visible that Rayleigh waves have a dispersive nature [19]. The group wave velocity was not precisely determined, but the transit time was estimated as that for halfspace. The direct longitudinal wave L and its diametrically reflected sequence $3L$ can be easily identified for ratio $b/a = 0$. For greater ratios, they are obviously blocked by the air-filled hole along their ray paths due to the large difference in acoustic impedance.

Therefore, this L wave is replaced by another longitudinal wave marked P in Figure 2a with a ray path shown in Figure 3a. According to Huygens's law, this ray path projects, in its shortest traveling distance, from the source on the inner hole at the tangent direction with $\theta = \cos^{-1}(b/a)$, and then climbs as a skimming L wave along the circular surface, and finally reaches the detection point along a symmetrical tangent direction. Due to the wide projection angle of the longitudinal directivity [6] for this regime, this wave is further broadened by this air-filled hole. According to Huygens' law, this air-filled hole will act as a second acoustic source which might produce various wave modes as longitudinal and shear waves marked as C in Figure 2a. The possible ray paths for C wave are shown in Figure 3b. The C wave could be regarded as the conversion of bulk wave between longitudinal and shear waves. In addition, wave $3L$ visible for the rod, $b = 0$, does not exist for any tubes as the hole blocks its back-forth ray trajectory.

The circumferentially reflected longitudinal waves ($2P$, $3P$) marked in Figure 2 have the corresponding ray trajectories shown in Figure 3c. The path for $2P$, $3P$ waves are blocked when $b/a > \tan(45°)$ and $\tan(60°)$, respectively. It is thus reasonable that the $2P$ wave is not visible for $b/a = 0.8$, while the $3P$ wave is still observable for this case. Similar phenomenon happens for their shear

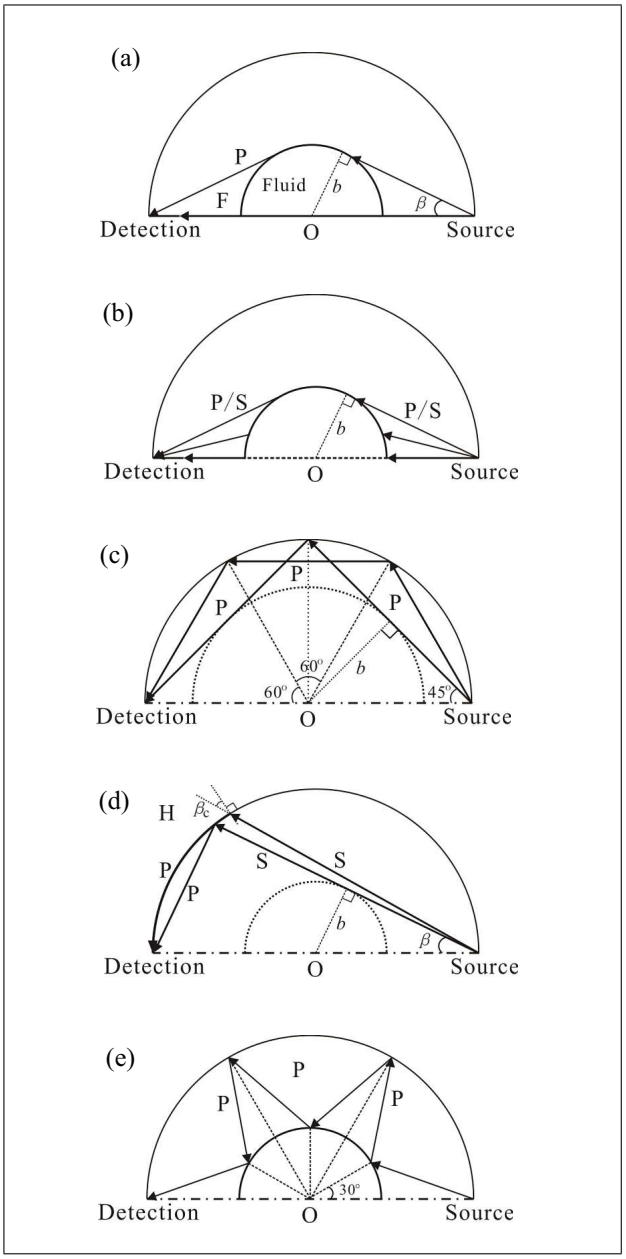

Figure 3. Ray trajectories of (a) direct L and deviated P longitudinal waves, (b) conversion C wave, (c) reflected $2P$, $3P$ longitudinal waves, (d) head (H) and converted waves, (e) guided $6P$ wave. Here β_c is the critical angle for the transverse wave path. β is an angle related to the transverse wave path. P denotes the longitudinal path, and S symbolizes the transverse or shear wave path.

counter parts (see the circumferentially reflected shear waves ($2S$, $3S$) marked in Figure 2). For the same reason, the further reflected shear wave $4S$ is discernible for all cylinders. The marked nP and nS represent the longitudinal and shear waves propagating along the outer circumference as lateral or skimming waves when the number of the relative paths n turns to infinite. Both waves nP and nS are not visible because no generation occurs at this radiation angle of 90° according to the directivity diagram for the ablation generation regime [6].

Table I. Ray paths and their corresponding normalized times of flight.

	Ray path	t/t_L
L	Longitudinal wave with a straight line from source to detection shown in Figure 3a	1
$2P$	Longitudinal wave reflected once at the external tube surface shown in Figure 3c	$\sqrt{2}$
$3P$	Longitudinal wave reflected twice at the external tube surface shown in Figure 3c	1.5
nP	Longitudinal wave infinitely reflected at the external tube surface	$\pi/2$
PS	Conversion of shear wave to longitudinal wave at the free surface	$V_L/V_S \cos\beta + \sin\beta,\ \beta = \tan^{-1}(V_S/V_L)$
H	Head wave resulted by the critical incidence of traverse wave	$V_L/V_S \cos\beta_c + \beta_c,\ \beta_c = \sin^{-1}(V_S/V_L)$
$2S$	Shear wave reflected once at the external tube surface	$\sqrt{2}V_L/V_S$
$3L$	Longitudinal wave reflected twice with a straight line from source to detection	3
$3S$	Shear wave reflected twice at the external tube surface	$1.5V_L/V_S$
$4S$	Shear wave reflected three times at the external tube surface	$4\sin(\pi/8)V_L/V_S$
nS	Shear wave infinitely reflected at the external tube surface	$0.5\pi V_L/V_S$
R	Surface wave propagating along the external surface	$\pi V_L/V_R$

The converted (PS) and head (H) waves, resulting of mode conversion at the outer circumference, have the corresponding ray trajectories shown in Figure 3d. The path for PS wave is blocked when $b/a \sin(\beta)$ ($\beta = \tan^{-1}(V_S/V_L)$], and it also happens for H wave when $b/a > \sin(\beta_c)$ ($\beta_c = \sin^{-1}(V_S/V_L)$). As marked in Figure 2a, the PS wave is hardly visible for $b/a = 0.6$ and 0.8. The H wave is observable for $b/a = 0.4$, but hardly visible for $b/a = 0.6$ and 0.8. The other visible singularities in the waveforms unmarked in Figure 2 are mainly bulk longitudinal and shear waves resulting of the reflection at both the inner and outer surfaces, since their time arrivals vary with the ratio b/a. As the thickness of the tube becomes small, the guided waves appear. The marked $6P$ wave clearly appears when $b/a = 0.6$, it is reflected by both inner and outer circular surfaces as displayed by its ray trajectory in Figure 3e. The unmarked bulk waves for $b/a = 0.8$ are mainly guided waves with complicated ray paths, but still clearly separated in the time domain.

Now, ultrasounds excited under the thermoelastic regime are considered in Figure 2b. Since the generation of Rayleigh wave is less dependent on the directivity than the generation of bulk longitudinal and transverse waves, Rayleigh wave with as large amplitude and dispersive nature is observed as that for the ablation regime. But the directivities of longitudinal and shear waves for this regime are quite different from that for the ablation regime [6]. As there is no radiation of longitudinal wave at the observation angle θ of 180°, the L and $3L$ waves for a rod, and P and C waves for air-filled tubes observed for the ablation regime are totally inexistent. Although waves $2P$, $3P$, $2S$ and $3S$ still exist for the thermoelastic regime, their amplitudes are less than their counterparts for the ablation regime, due to the small amplitude in the corresponding directivity. Similarly, the change of the amplitude for the PS and H waves is in agreement with the difference of the corresponding directivity of the two regimes. These differences further emphasize the effectiveness of the theoretical solution given in the previous section.

Moreover, the displacement waveforms shown in Figure 2a and b for both regimes are respectively identical to that calculated by a previous theory treating the inner of tube as a vacuum (See Figure 2 in [11]). This coincidence further implies the validness of both models in section 2 and in [11] as the effects of the filling in by air could be neglected.

5. Ultrasounds excited in glycerol-filled tubes

To further demonstrate the accuracy of the theoretical solution in section 3, the radial surface displacements are calculated for glycerol-filled aluminum tubes with the same velocities of longitudinal and shear waves, and the same density, at an observation angle θ of 180°. Corresponding displacements to Figure 2 for four tubes with the same dimensions are shown in Figure 4 for both regimes. The velocity and density considered for glycerol ($C_3H_8O_3$) are $V_F = 2200$ m/s and $\rho_F = 1260$ kg/m^3 at the room temperature of 22 °C [21]. Here water was not chosen since it has less acoustic impedance match to aluminum than glycerol. The corresponding results for an aluminum rod (a=5 mm and b=0) is again displayed in Figure 4 for the purpose of comparison.

First, interest is focused on ultrasounds excited under the ablation regime in Figure 4a. The same vertical scale treatment is made owing to the very large amplitude of the

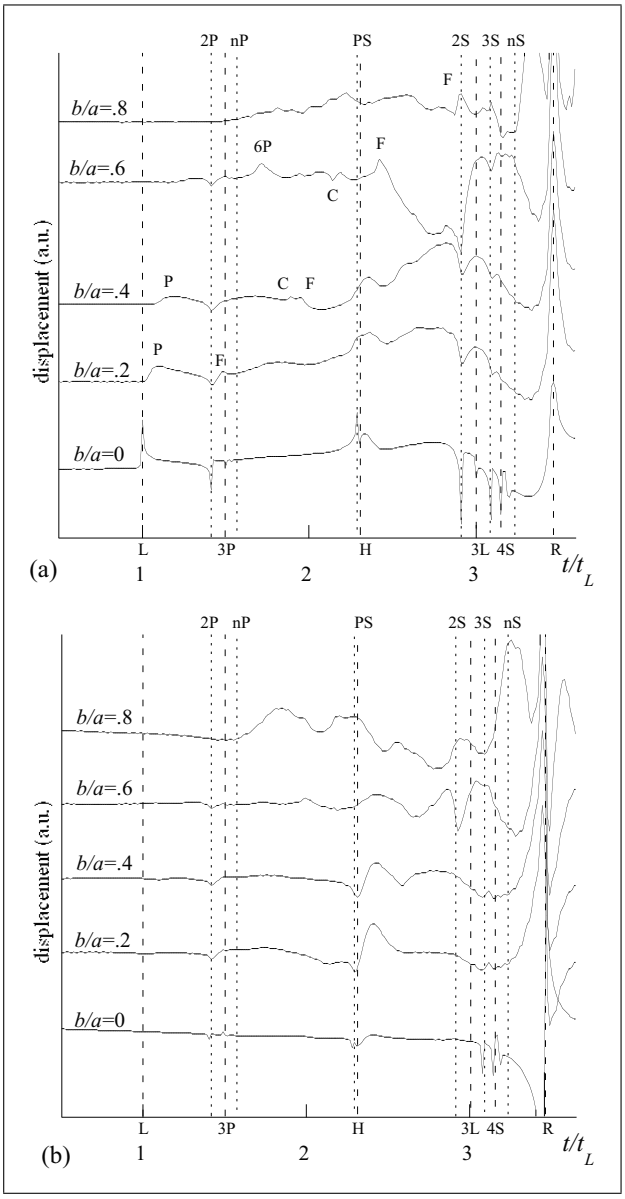

Figure 4. Displacements calculated at an observation angle $\theta = 180°$ of the laser line source generation under either the ablation (a) or the thermoelastic (b) regime for glycerol-filled tubes with various b/a ratios of 0, 0.2, 0.4, 0.6, and 0.8. Symbols at the top or bottom of each dashed line respectively denote the wave marked by the dense or sparse dashed line.

cylindrical Rayleigh wave. Again, waves marked as P and C described in the previous section are observed due to the combinated effects of the inner circular interface and to the directivity of ablation generation. The same phenomenon is also observed for the circumferentially reflected longitudinal ($2P$, $3P$, nP) and shear ($2S$, $3S$, nS) waves discussed in the previous section, since the existence of the fluid does not affect the generation directivity and the corresponding ray trajectories. This also happens for the converted (PS) and head (H) waves shown in Figure 4.

However, the direct longitudinal wave passing through the fluid appears for the four tubes as marked by symbol F in Figure 4a. It has the ray trajectory shown in Figure 3a. Its amplitude is affected by the difference of the acoustic impedance between the solid and fluid. And its arrival time is just determined by the size of the hole and the sound velocity in the fluid. It is observable that the unmarked singularities of the waveform for $b/a = 0.8$ in Figure 4a have less amplitudes than their counterparts of the air-filled tubes (see Figure 2a). The guided waves reflected by both circular surfaces are affected by the filled fluid, since they transmit part of their energy to the fluid at the solid-fluid interface.

Now, ultrasounds excited under the thermoelastic regime are considered in Figure 4b. Since the generation of Rayleigh wave depends less on the directivity than that of bulk longitudinal and shear waves, same phenomenon is observed for the ablation regime. But the directivities of longitudinal and shear waves for this regime are quite different from that for the ablation regime [6]. As there is no radiation of longitudinal wave along this observation direction ($\theta = 180°$), the L and $3L$ waves for a rod and P and C waves for glycerol-filled tubes observed for the ablation regime are totally inexistent. Moreover, the F wave signifying the existence of the fluid for the ablation regime has now totally disappeared for this thermoelastic regime. Although waves generated by this radiation like $2P$, $3P$, $2S$, and $3S$ still exist, their amplitudes are less than their counterparts for the ablation regime, due to the small amplitude in the corresponding directivity. Similarly, the change of the amplitude for the PS and H waves is in agreement with the difference of the corresponding directivity of the two regimes. These differences further emphasize the accuracy of the theoretical solution of the previous section.

6. Comparison to experiments

To further validate the physical model and theoretical solution, a Nd:YAG laser was used delivering pulses of 10 ns duration at a wavelength of 1064 nm. The laser excitation beam was focused to a line of length 4 cm and width 0.1 mm by a cylindrical lens. An interferometer [14] of a bandwidth 120 MHz, a power 100 mW and sensitivity 10^{-14} m/$\sqrt{\text{Hz}}$ was used to detect the radial displacement of the surface at an observation angle of $\theta = 180°$. The signal was averaged over 15 shots for the ablation generation and 110 shots for the thermoelastic generation. The laser energy for the ablation generation is about 50 mJ, and is about 5 mJ for the thermoelastic generation, so providing power densities in each side of the ablation threshold [6]. The experimental waveforms were obtained for an air or a glycerol-filled aluminum tube of external radius $a = 5$ mm and internal radius $b = 1.5$ mm. Corresponding numerical waveforms are calculated with the theoretical solution derived in section 3, and they are also presented for the purpose of comparison.

First, interest is focused on ultrasounds excited in an air- filled tube under ablation generation. As shown in Figure 5a, the calculated waveform is in good agreement with

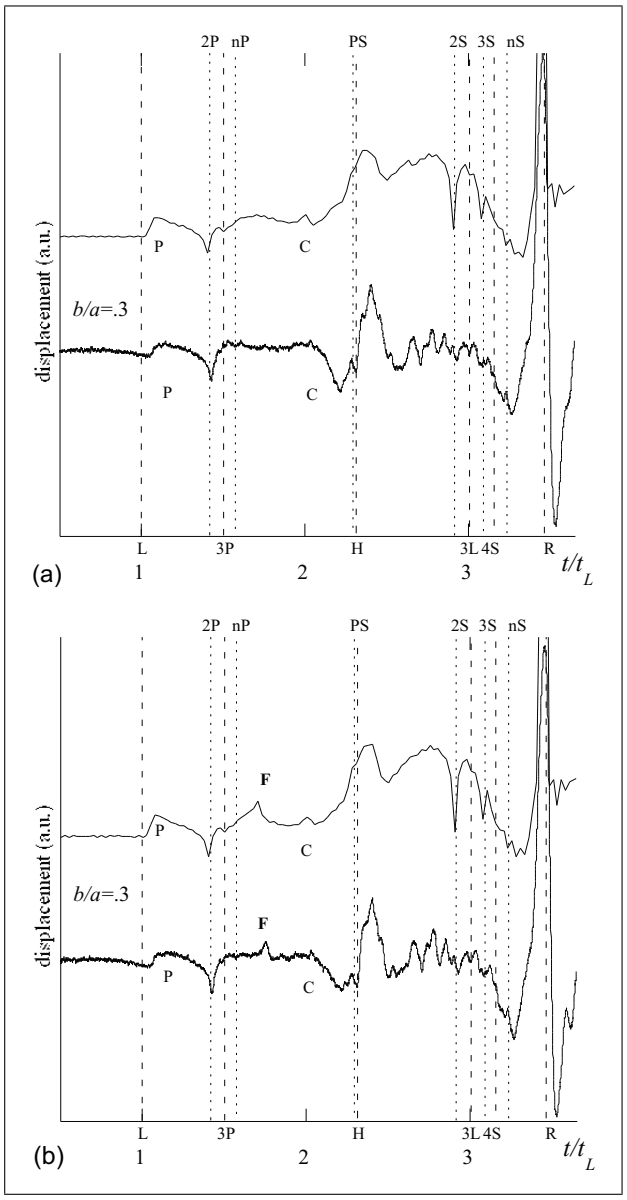

Figure 5. Displacements calculated (top) and detected (bottom) at an observation angle $\theta = 180°$ in a tube of b/a ratio 0.3 without (a) or with (b) glycerol for the ablation generation. Symbols nearby the singularities of the waveform denote possible wave arrivals.

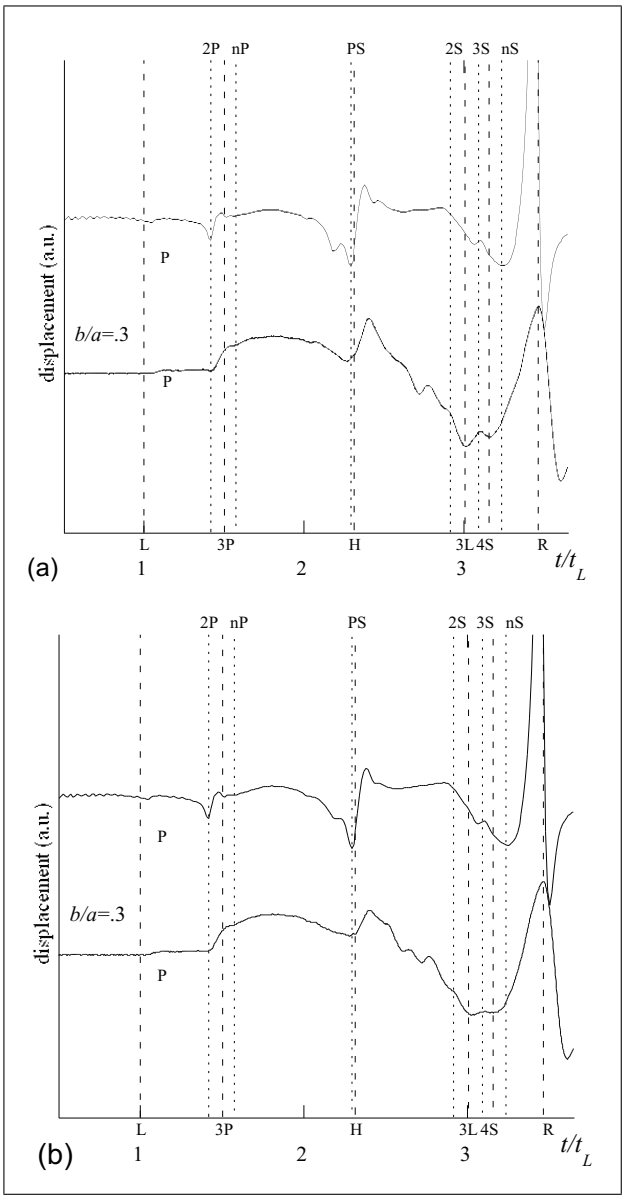

Figure 6. Displacements calculated (top) and detected (bottom) at an observation angle $\theta = 180°$ in a tube of b/a ratio 0.3 without (a) or with (b) glycerol for the thermoelastic generation. Symbols nearby the singularities of the waveform denote possible wave arrivals.

the experimental result in the time arrival, shape and relative amplitude of various longitudinal ($P, 2P$) bulk waves, conversion bulk waves (C) and head wave (H). Here the R waves are clearly visible with large amplitudes. Due to the finite length and width of the actual line source, and to the experimental noise, the $2S$ wave could not be clearly identified in the experimental waveform.

Now, interest is focused on ultrasounds excited in a glycerol-filled tube with the same dimensions. As shown in Figure 5b, the calculated waveform is also in good agreement with the experimental result in the time arrival, shape and relative amplitude of the direct longitudinal wave passing through the liquid (F), various longitudinal ($P, 2P$) bulk waves, conversion bulk waves (C) resulting of mode conversion at the inner circumference, and head wave (H) resulting of mode conversion at the outer circumference. The existence of F wave further emphasizes the effectiveness of the physical model in section 2 and the corresponding theoretical solution in section 3. To further validate the findings, similar results are compared for the air-filled and glycerolfilled tube under the thermoelastic regime. As shown in Figures 6a and 6b, good agreement is also found for the calculated and experimental waveforms in the time arrival, shape and relative amplitude of various longitudinal ($P, 2P$), and conversion bulk waves (C), and head wave (H).

Again, due to the finite length and width of the actual line source, and to the experimental noise, the 2S wave

could not be clearly identified in the experimental waveform [21]. Since the source directivity diagram for the thermoelastic regime shows that no radiation of longitudinal wave is expected at the observation angle θ of 180° for this thermoelastic regime, the disappearance of the F wave further emphasizes the validness of both theoretical modeling and experimental finding.

7. Conclusion

A physical model and corresponding solution are presented to calculate the transient response of a fluid-filled tube excited by a laser line pulse. The theoretical solutions are demonstrated by transient displacements of air-filled and glycerol-filled tubes calculated and analyzed for various ratios of internal radius to external radius. Experimental displacements are obtained and compared for air-filled or glycerol-filled tubes under ablation and thermoelastic regimes. Agreements are observed in the time, shape and relative amplitude of the various longitudinal and transverse bulk waves propagating through the tube or reflected by the circular surfaces.

Acknowledgement

This work was done at Laboratoire de Mécanique Physique, Université Bordeaux 1. Y. Pan was supported by CNRS under PICS no. 3357 (International Programs for Scientific Cooperation). He is grateful to the hospitality of Laboratoire de Mécanique Physique, Université Bordeaux 1.

References

[1] M. C. Junger, C. Mass. Journal of Applied Mechanics **19** (1952) 439–445.

[2] D. C. Gazis. J. Acoust. Soc. Am. **31** (1959) 568–578.

[3] T. J. Plona, S. Kostek, S. Chang. J. Acoust. Soc. Am. **86** (1989) S119.

[4] X. Zhao, J. L. Rose. J. Acoust. Soc. Am. **115** (2004) 1912–1916.

[5] G. Liu, J. Qu. J. Acoust. Soc. Am. **104** (1998) 1210–1220.

[6] C. B. Scruby, L. E. Drain: Laser ultrasonics: Techniques and applications. Adam Hilger, New York, 1990.

[7] Y. Pan, C. Rossignol, B. Audoin. Appl. Phys. Lett. **82** (2003) 4379–4381.

[8] Y. Pan, C. Rossignol, B. Audoin. J. Acoust. Soc. Am. **117** (2005) 3600–3608.

[9] L. Tang, J. Cheng. J. Nondestructive Evaluation **21** (2002) 45–53.

[10] W. Gao, C. Glorieux, J. Thoen. J. Appl. Phys. **91** (2002) 6114–6119.

[11] Y. Pan, L. Li, C. Rossignol, B. Audoin, N. Chigarev. Ultrasonics **44** (2006) e843–e847.

[12] J.-Y. Kim, J.-G. Ih. Applied Acoustics **64** (2003) 1187–1204.

[13] P. S. Wilson, R. A. Roy, W. M. Carey. Acoustics Research Letters Online **2** (2001) 103–108.

[14] D. Royer, E. Dieulesaint. Proceedings of IEEE Ultrasonics Symposium, New York, 1986, 527–530.

[15] D. A. Hutchins. – In: Physical Acoustics, Vol. 18. Academic, New York, 1988, 21–123.

[16] L. R. F. Rose. J. Acoust. Soc. Am. **75** (1984) 723–732.

[17] Y. H. Berthelot, I. J. Busch-Vishniac. J. Acoust. Soc. Am. **81** (1987) 317–327.

[18] X. Wu, M. Qian, J. H. Cantrell. Appl. Phys. Lett. **83** (2003) 4053–4055.

[19] W. Hu, M. Qian. Chin. Phys. Lett. **21** (2004) 1294–1297.

[20] R. L. Weaver, W. Sachse, K. Y. Kim. J. Appl. Mech. **63** (1996) 337–339.

[21] CRC Handbook of chemistry and physics, 51st edition 1970–1971. The chemical rubber co., Cleveland, 1971.